Investigating Coupled Impacts of Climate Change and Socioeconomic Transformation on Desertification by Using Multitemporal Landsat Images: A Case Study in Central Xilingol, China

Shuang Li and Yichun Xie, *Member, IEEE*

***Abstract*—A case study is conducted in Xilingol Rangeland, Inner Mongolia, China, to investigate the driving factors of temporal dynamics of desertification by using time-series Landsat images. The spectral characters of sand dunes and urban lands in the arid and semiarid grassland environments are very similar, and thus, it is hard to discriminate them with traditional image classifiers. Nine available scenes of Landsat images without cloud cover from 1985 to 2010 are chosen for the case study. An object-oriented image classification (OOIC) is developed to classify sand dunes. The classification results are assessed with the ground reference points in 1985, 2004, and 2010, the land-cover maps produced from other classifiers in literature, and Google Earth historical aerial photo archives. Second, the areas of sand dunes derived from OOIC at the nine times are extrapolated into a 26-year time-series data set from 1985 to 2010 by applying several extrapolation techniques commonly used in regional geographic studies. Afterward, six climate factors and nine socioeconomic variables during the same study period along with the sand dune area are composed into a completed data set to investigate the coupled impacts of climate change and socioeconomic transformation on the temporal dynamics of desertification. Three types of regression models (climate model, economic model, and the coupled model) are explored, respectively, to examine which factors contribute more to the desertification dynamics. The findings confirm that the desertification process in Xilingol Rangeland is very complicated although it shows a strong causal relationship with several socioeconomic factors.**

***Index Terms*—Climate change, coupled human–nature system, desertification, object-oriented classification, time-series analysis.**

I. Introduction

DESERTIFICATION, which destroys land resources and reduces ecosystem services, is a very serious environmental, ecologic, and socioeconomic problem in the world [1]. Along with the socioeconomic development, China has seriously suffered from desertification in the past decades. Desertification has been worsened with an increasing annual rate in the last 50 years [2]. Therefore, it is an urgent task to dynamically monitor the temporal and spatial changes of desertification and to provide scientific data to the government for combating desertification.

Remote sensing techniques have been applied in monitoring the intrusion of sand dunes. There are various methods for processing remote sensing data and extracting sand dune distribution information. Traditional methods from remote sensing data rely on image-based vegetation indices such as normalized difference vegetation index, enhanced vegetation index, soil-adjusted vegetation index (SAVI), and modified SAVI to assess vegetation conditions [3]. Moreover, some indices can reflect vegetation patterns and spatial heterogeneity, such as the landscape connectivity index [4] and moving standard deviation (SD) index [5]. However, the spectral signatures of sand dunes are often mixed with other land covers. It is important to examine the optical properties of sand dunes and other land-cover/land-use types in order to differentiate sand dunes from the others [6]. The key to the success of extracting sand dunes from remotely sensed images is to determine those spectral bands that are capable of distinguishing the signatures of sand dunes.

Another noteworthy point is that desertification generally results from climatic variations, human activities, and their interplay [1]. It has been controversial which factors (climatic or socioeconomic) have direct impacts on or contribute more to desertification and whether the climatic and the socioeconomic factors differ or interact together to affect the dynamic process of desertification. The objective of this letter is to develop techniques for assessing and analyzing the impacts of coupled climatic and socioeconomic factors on desertification process with a case study in central Xilingol League, Inner Mongolia, China.

II. Study Area and Data Preprocessing

The study area is located in the middle portion of Xilingol League, Inner Mongolia, China. It is a large piece of natural grassland closest to Beijing and acts as an important belt to protect North China from dust storms. On average, the growing season is from late April to August. Grassland covers 97.3% of land area, with the dominant types of *Stipa grandis* steppe and *Aneurolepidium chinense* steppe. The study area includes 12 gazha (villages), 2 pastures, and 1 city (see Fig. 1).

Manuscript received January 27, 2013; revised March 17, 2013; accepted March 26, 2013. This work was supported in part by Land-Cover/Land-Use Program at the National Aeronautics and Space Administration under Grant NNX09AK87G. *(Corresponding author: Y. Xie.)*

S. Li is with the International School of Software, Wuhan University, Wuhan 430079, China (e-mail: lishuang129@gmail.com).

Y. Xie is with the Department of Geography and Geology, Eastern Michigan University, Ypsilanti, MI 48197 USA (e-mail: yxie@emich.edu).

Color version of one or more of the figures in this paper are available online at http://ieeexplore.ieee.org.

Digital Object Identifier 10.1109/LGRS.2013.2257158

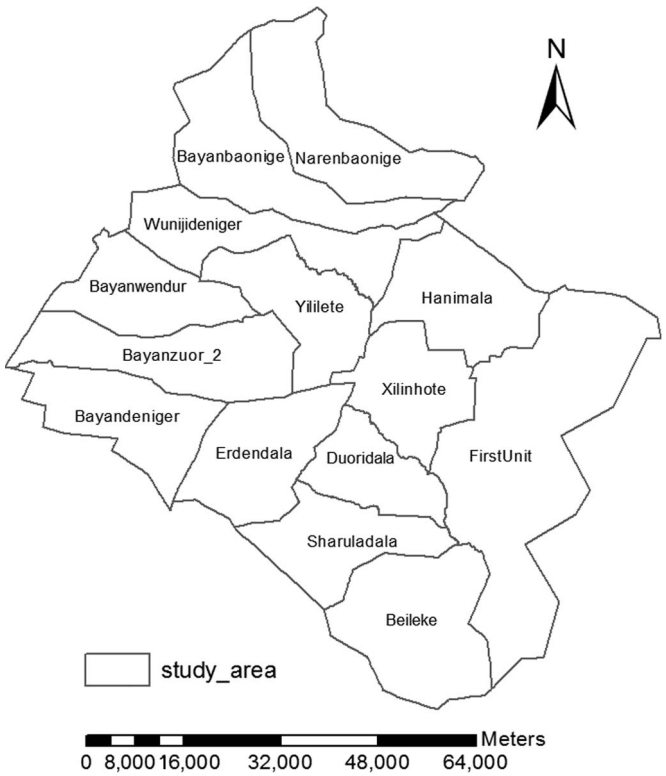

Fig. 1. Administrative composition of the study area.

A nine-year time series (1985, 1989, 1991, 1995, 2000, 2004, 2006, 2007, and 2010) of Landsat TM/ETM+ was collected. The study area was fully covered by the mosaic of Landsat images from Row 29 to Row 30 of Path 124. All TM/ETM+ data were collected in summer (mainly in July and August) for monitoring the long-term processes of desertification. As the images in 2006 and 2010 were from the ETM+ sensor with the scan-line corrector off, the gaps in the two images were filled using the localized linear histogram match method [7]. Then, all images were geometrically registered by the second-order polynomial geometric registration with 12 ground control points that were evenly distributed over the images. Furthermore, all images were nearest neighborhood resampled to 30-m spatial resolution and projected onto the WGS 84 datum with the UTM (Universal Transverse Mercator, 50-N) projection. The geometrical registration precision was within 0.5 pixel. Finally, in order to reduce the influence of the reflectance variation among the images acquired at different times, the relative radiometric correction was performed to yield the normalized radiometric data on a common scale. Histogram match was used to carry out the relative radiometric correction. The histograms of all other images were matched to the image in 1985.

III. Methodology

A. Spectral Characteristic Analysis of Land Covers/Uses

The Landsat TM 5/ETM+ multispectral image provides seven bands in the spectrum of blue, green, red, near-infrared, mid-infrared with 30-m spatial resolution (bands 1–5 and 7), and a thermal infrared channel with 120 m/60 m spatial resolution (band 6). Band 6 is not used in the analysis due to the different spatial resolution and large spectral wavelength.

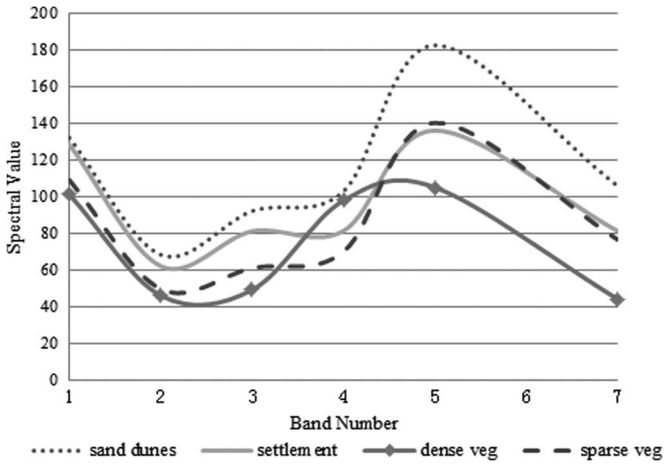

Fig. 2. Spectral curves of Landsat TM/ETM+ images.

To analyze the spectral differences between the sand dunes and other land covers/uses, we sampled four typical types of land covers/uses (see Fig. 2). The mean value of sand dunes in band 5 was the largest, whereas the mean value of settlement was the third. The mean values of vegetation covers in bands 1, 2, and 3 were lower than those of sand dunes and settlement. The spectral signatures of sand dunes and settlement were mixed in band 7.

To make use of the mean spectral values of the bands, the normalized difference between two bands (NDTB) for each land-cover/use type was computed using the following equation:

$$NDTB = (band_i - band_j)/(band_i + band_j), \quad i \neq j \quad (1)$$

where i and j are the band numbers. There are 15 combinations of two-band difference $NDTB_{i,j}$ for the six bands. Let $d_{m,n}$ be the difference value of $NDTB_{i,j}$ between a pair of land-cover/use types, m and n. The maximum $d_{m,n}$ was used to distinguish two land-cover/use types, m and n. For instance, the value of $NDTB_{1,5}$ was the highest for $d_{\text{sand dunes,settlement}}$. Thus, $NDTB_{1,5}$ was selected for distinguishing sand dunes from settlement. In the similar way, the normalized difference of bands 4 and 7 $NDTB_{4,7}$ was selected for separating sand dunes and dense vegetation. The normalized difference of bands 1 and 3 $NDTB_{1,3}$ was selected for differentiating sand dunes and sparse vegetation.

B. OOIC

Based on the analysis of the spectral features of the sand dunes and other land covers/uses, we developed an object-oriented image classification (OOIC) to extract sand dunes. The image objects were obtained by the multiresolution segmentation method, which was a bottom-up region-merge process starting with one-pixel objects and small regions. These objects were gradually merged to form big ones. The stop criteria were the minimum growth of homogeneity inside objects and the maximum growth of heterogeneity between objects. The multiresolution segmentation was conducted in Definiens software.

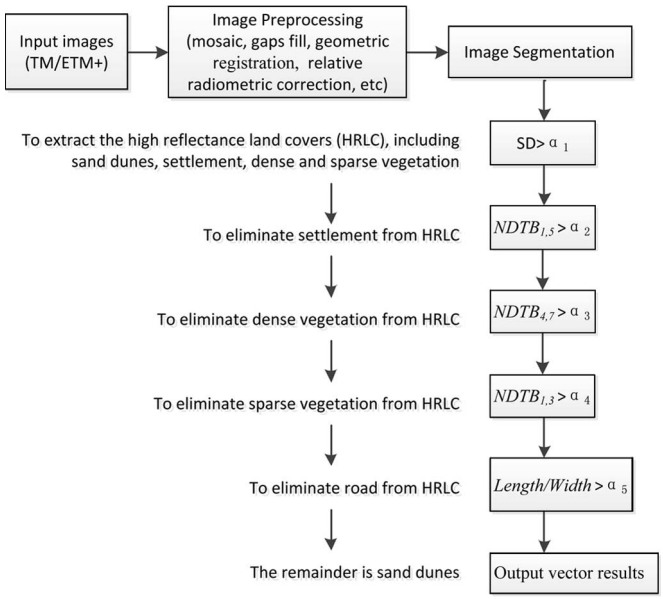

Fig. 3. OOIC for extracting sand dunes.

The SD was calculated from the layer values of all pixels to form an image object, which was used to extract the high-reflectance land covers (HRLCs). According to the spectral analysis in Section III-A, $NDTB_{1,5}$, $NDTB_{4,7}$, and $NDTB_{1,3}$ were used to eliminate the settlement, the dense vegetation, and the sparse vegetation from HRLC. The flowchart of OOIC for extracting sand dunes is shown in Fig. 3. First, a nine-year time series of Landsat TM/ETM+ images was preprocessed, including mosaic, gap filling, geometric registration, and relative radiometric correction, as described in Section II. Then, the preprocessed images were segmented by using the multiresolution segmentation. Once the images were segmented, the image objects were obtained and the object features were calculated for classification. The image objects with SD values larger than α_1 ($\approx$2.5) were classified as HRLCs, including sand dunes, settlement, and dense and sparse vegetation. If $NDTB_{1,5}$ value was larger than α_2 (≈ -0.12), the image object was classified as settlement. If $NDTB_{4,7}$ value was larger than α_3 ($\approx$0.14), the image object is classified as dense vegetation. If $NDTB_{1,3}$ value was larger than α_4 ($\approx$0.22), the image object was classified as sparse vegetation. If the length/width ratio was larger than $\alpha_5 (= 5)$, the image object was classified as road. The remainder in HRLC was classified as sand dunes.

The classification accuracy was assessed in three ways. First, 140 random ground reference points (GRPs) were selected from the GRPs acquired in 1985, 2004, and 2010, which were available through our other projects [8], [9], [13] to validate the classification outcomes. Second, since the lack of GRPs in other six years was a limitation, manual checking of the OOIC classification results in these six years was conducted with the high-resolution images found in Google Earth historical archives. Third, the OOIC classifications in 1985, 2004, and 2010 were also compared with the land-use/cover maps obtained through our other projects [8]–[10]. The last two complementary methods confirmed that the accuracy assessment of the nine-year OOIC classification by using one set of testing GRPs in our case study was reliable. The overall accuracy and Kappa coefficient defined by the error matrices were used as the measures for accuracy assessment. The accuracy assessment results of our OOIC were very high (see Table I), which met the general accuracy requirement of land-cover/use change detection studies [8], [9]. From Table I, it is shown that the overall accuracy and Kappa coefficient show comparable accuracy levels. In particular, Kappa coefficient reflects the difference between the actual agreement and the agreement expected by chance. A Kappa value of 0.80 means there is 80% better agreement than by chance alone. The higher is a Kappa value, the higher is the confidence concerning the accuracy assessment.

TABLE I
AREA OF SAND DUNES*

Year	Sand dunes Area (km^2)	Overall Accuracy	Kappa Coefficient
1985	469.5	0.929	0.882
1989	578.3	0.929	0.883
1991	572.9	0.907	0.847
1995	639.3	0.936	0.894
2000	697.7	0.893	0.823
2004	416.6	0.921	0.870
2006	406.4	0.907	0.848
2007	425.9	0.907	0.847
2010	595.7	0.921	0.871

** The total area of the study area is 4797.65 km^2*

C. Extrapolating the Nine Years of the Sand Dunes Data Into 26 Years

Several local population and economic extrapolation methods [10], [11] such as linear, log–linear, exponential, geometric, Gompertz, and parabolic were applied to extrapolate the nine-year data to a 26-year data set. Since each of these extrapolation methods reflected one statistical trend, none of them would fit to the fluctuations demonstrated by the nine-year values of sand dunes. In other words, none of these methods would produce a reliable result if an extrapolation method was exercised over the entire study period. In order to identify the change trend, the nine-year classified results of sand dunes were plotted (marked x) in Fig. 4. The change tendency, which was graphically revealed, suggested two possible ways of extrapolation. First, the study period could be separated into three subperiods by four years, i.e., 1985, 2000, 2006, and 2010, and then a linear extrapolation could be applied to the three subperiods, respectively, to fit a curve of sand dune change. Second, the study period could be dissected at year 2000 into two subperiods, i.e., 1985–2000 and 2000–2010. A linear extrapolation could be applied over 1985–2000, whereas a parabolic curve fitting could be done over 2000–2010. As a matter of fact, both extrapolation outcomes were almost identical due to the short time spans of the subperiods. Although the outcome from the first extrapolation approach was selected to construct the 26 years of sand dune change vector data for exploring the driving factors of desertification, it is important to iterate that

[1]The solid x symbols indicate the classified values of sand dunes, whereas the dots linearly connect these values. The units on the Y-axis are different for different factors.

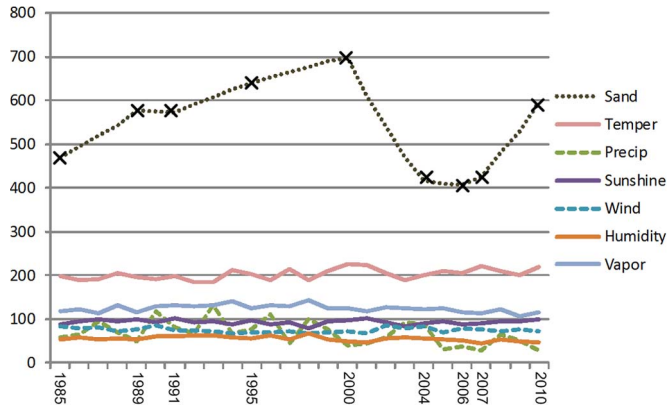

Fig. 4. Extrapolating the areas of sand dunes from 9 to 26 years.[1]

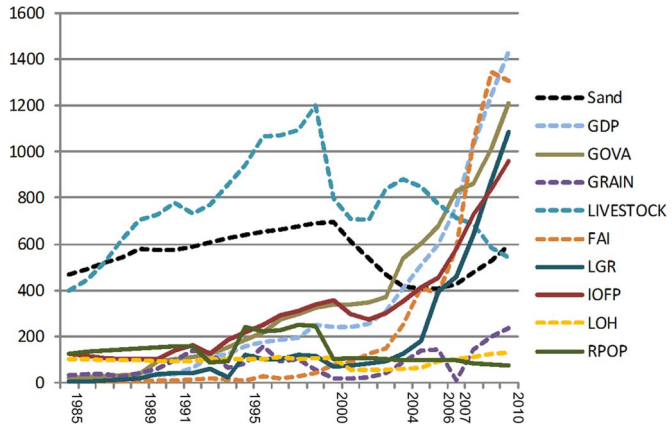

Fig. 5. Scatter plots of nine socioeconomic factors and the sand dune area.[2]

the extrapolation of sand dune areas over the 26-year period was cross validated between two different approaches. Furthermore, the time-series change of sand dunes exhibited a distinct temporal dynamics, gently increasing 1985–2000, dramatically declining 2000–2005, and considerably climbing 2005–2010.

D. Exploring Which Factors Contribute More to the Desertification Process

Nine socioeconomic factors (see Fig. 5), namely, gross domestic product (GDP); gross output value of farming, forestry, animal husbandry, and fishery (GOVA); grain output (GRAIN); the amount of the livestock by the end of the year (LIVESTOCK); fixed assets investment (FAI); local government revenue (LGR); per capita net income of farmers and pastoralists (IOFP); the total length of highways (LOH); and rural population (RPOP), from 1985 to 2010 were collected along with the extrapolated areas of sand dunes and the six climatic factors to create a complete data set to investigate the coupled impacts of climate change and socioeconomic transformation on desertification. Three types of regression models were analyzed.

1) Climate model—The sand dune area was regressed against six climatic factors.
2) Economic model—The sand dune area was against nine socioeconomic factors.

[2]The units on the Y-axis are different for different factors.

TABLE II
RESULT OF REGRESSION ANALYSIS ON THE COUPLED CLIMATIC AND SOCIOECONOMIC DATA SET

Regression Statistics	
Multiple R	0.9606
R Square	0.9228
Adjusted R Square	0.7856
F	6.7265
Significance F	0.0032

	Coefficients	*t Stat*	*P-value*
Intercept	-1276.8430	-0.7415	0.4773
Humidity	19.1352	0.7354	0.4808
Vapor	-7.3289	-0.6562	0.5281
Temper	6.4784	0.7358	0.4806
Precip	0.1030	0.1397	0.8920
Sunshine	2.6442	0.8144	0.4364
Wind	-0.4505	-0.1623	0.8746
GDP	-0.1221	-1.7077	0.1219
GOVA	**-0.8959**	**-2.3883**	**0.0407**
GRAIN	-0.0205	-0.5712	0.5818
LIVESTOCK	0.4819	1.5994	0.1442
FAI	0.0004	0.0152	0.9882
LGR	**0.1252**	**2.5294**	**0.0323**
IOFP	**1.7120**	**3.5125**	**0.0066**
LOH	-1.0756	-0.8170	0.4350
RPOP	**-1.1172**	**-2.1426**	**0.0608**

3) Coupled model—The sand dune area was against all 15 variables.

Because the climate factors and the sand dune change displayed dissimilar trends (see Fig 4), the climate model did not find that any climate factor was linearly correlated to the sand dune area change statistically at the 5% confidence level. In other words, the desertification process showed a nonlinear relationship with the climate factors. The economic model found out that six socioeconomic factors, i.e., IOFP, LGR, RPOP, LIVESTOCK, GOVA, and GDP, in a decreasing order had significant impacts on desertification statistically with the R-square 0.8847. The coupled model produced the best fit model based on R-square 0.9228 and identified four factors, i.e., IOFP, LGR, RPOP, and GOVA, which contributed most to the desertification process in the study area (see Table II). It was easily understood that the sand dune expansion was significantly correlated with the increase in IOFP and LGR. This finding confirms that the increased income and revenue were largely depending on intensified utilization of grassland, which often led to desertification. On the other hand, the sand dune land cover displayed negative relationships with RPOP and GOVA. When we looked at the data, we found that rural population witnessed noticeable fluctuations in the past 26 years (see Table III), which was consistent with the national trend of the floating population in China [12]. Especially in the

TABLE III
FLUCTUATIONS OF RURAL POPULATION

Year	1985	1986	1987	1988	1989	1990	1991	1992	1993
RPOP*	127.5	134.5	140.8	146.2	150.8	154.6	157.7	159.9	89.0
Year	1994	1995	1996	1997	1998	1999	2000	2001	2002
RPOP*	92.0	242.0	225.0	226.0	253.0	247.0	105.0	106.0	107.7
Year	2003	2004	2005	2006	2007	2008	2009	2010	
RPOP*	101.9	98.1	98.5	98.0	97.0	84.4	79.2	76.4	

recent years, rural population dramatically declined, which apparently alleviated the pressures of grazing and farming on the grassland and thus deterred the desertification process.

IV. ANALYSIS AND CONCLUSION

The longitudinal change of sand dune areas 1985–2010 was significant, showing clear trends that were not consistent with the changing patterns of six climatic factors (see Fig. 4). Precipitation showed noticeable fluctuations while the remaining climate factors were oscillating around their average values, respectively. It was very hard to make informative judgments of their long-term tendencies based the 26 years of observations. Therefore, it was apparent that there were no linear correlations between the desertification process and the climate changes. On the contrary, it was interesting to find out that the nine socioeconomic variables displayed dramatically varied change patterns (see Fig. 5). Among them, four to six scatter plots were somehow following the trend of the sand dune area changes. As a result, four to six of these socioeconomic variables significantly explained the variation of the sand dune area changes statistically (see Table II). This finding helps to clarify some myths about the impacts of climate changes on ecological systems. First, it would be a wrong assumption that there existed a simple causal relation between the desertification and the climate changes. Second, comparing the graphic correspondence and the statistical nonlinearity between the climate factors and the sand dune area change, it easily led to a suggestion that it would take a much longer period of observation to investigate the relationship between the desertification dynamics and the climate changes. Third, on the contrary, the human activities could play a significant role of driving the desertification process or ecological degradation in Xilingol Rangeland at a relatively short period (1985–2010 in this case study) [13]. Fourth, although there was no linear relationship between the climate factors and the sand dune area change, the inclusion of the climate factors in the regression analysis of the coupled climatic and socioeconomic data set significantly changed the regression outcome. The R-square was changed, and two economic variables were no longer statistically contributing to the desertification process.

Finally, this paper has confirmed its original intention that the integration of remote sensed data with the climatic and socioeconomic data could help study complex interactions between natural and human systems. Because of the availability of relatively long archives of satellite images, it is feasible to construct the time-series data sets with adequate image processing and data extrapolation techniques. Although the methods tested in this paper are limited and the case study area is not too large, the approach has illustrated bright potentials.

REFERENCES

[1] Z. Adeel, U. Safriel, D. Niemeijer, and R. White, "Ecosystems and human well-being: Desertification synthesis," World Resources Inst., Washington, DC, USA, 2005.
[2] T. Wang, Z. Zhu, and W. Wu, "Sandy desertification in the north of China," *Sci. China Ser. D, Earth Sci.*, vol. 45, no. Suppl. 1, pp. 23–34, Dec. 2002.
[3] T. Wang, G. T. Chen, H. L. Zhao, Z.-B. Dong, X.-Y. Zhang, X.-J. Zheng, and N.-A. Wang, "Research progress on aeolian desertification process and controlling in north of China," *J. Desert Res.*, vol. 26, no. 4, pp. 507–516, Jul. 2006.
[4] D. Sun, R. Dawson, H. Li, R. Wei, and B. Li, "A landscape connectivity index for assessing desertification: A case study of Minqin County, China," *Landscape Ecol.*, vol. 22, no. 4, pp. 531–543, Apr. 2007.
[5] R. Jafari, M. M. Lewis, and B. Ostendorf, "An image-based diversity index for assessing land degradation in an arid environment in South Australia," *J. Arid Environ.*, vol. 72, no. 7, pp. 1282–1293, Jul. 2008.
[6] M. Dawelbait and F. Morari, "Limits and potentialities of studying dryland vegetation using the optical remote sensing," *Italian J. Agron.*, vol. 3, no. 2, pp. 97–106, 2008.
[7] P. Scaramuzza, E. Micijevic, and G. Chander, "SLC gap-filled products: Phase one methodology," Landsat Technical Notes 2004.
[8] Y. Xie, Z. Sha, and Y. Bai, "Classifying historical remotely sensed imagery using a tempo-spatial feature evolution (T-SFE) model," *ISPRS J. Photogramm. Remote Sens.*, vol. 65, no. 2, pp. 182–190, Mar. 2010.
[9] Z. Sha, Y. Bai, Y. Xie, M. Yu, and L. Zhang, "Using a hybrid fuzzy classifier (HFC) to map typical grassland vegetation in Xilin River Basin, Inner Mongolia, China," *Int. J. Remote Sens.*, vol. 29, no. 8, pp. 2317–2337, Apr. 2008.
[10] S. K. Smith, J. Tayman, and D. A. Swanson, *State and Local Population Projections*. Norwell, MA, USA: Kluwer, 2001.
[11] R. E. Klosterman, *Community Analysis and Planning Techniques*. Lanham, MD, USA: Rowman & Littlefield Publ Inc., 1990.
[12] C. Duan and G. Yang, "Trends in destination distribution of floating population in China," *Population Res.*, vol. 33, no. 6, pp. 1–12, 2009.
[13] Y. Xie and Z. Sha, "Quantitative analysis of driving factors of grassland degradation: A case study in Xilin River Basin, Inner Mongolia," *Scientific World J.*, vol. 2012, pp. 169 724-1–169 724-14, Apr. 2012.